Fuel Processing Technology 92 (2011) 1587–1592
doi:10.1016/j.fuproc.2011.04.002

Removal of hydrogen sulfide using red mud at ambient conditions

Ramesh Chandra Sahu [a], Rajkishore Patel [a] and Bankim Chandra Ray [b]

[a] Department of Chemistry, [b] Department of Metallurgical and Materials Engineering
National Institute of Technology, Rourkela 769008, Orissa, India
E-mail address: rcsahu.chem@gmail.com

Abstract

Red mud (RM) is a caustic waste product of alumina industry. A laboratory study was conducted to investigate the removal of hydrogen sulfide (H_2S) gas using RM at ambient conditions. Red mud was characterized before reaction and after reaction by using XRD, BET, SEM/EDX, TG-DSC, FT-IR, and CHNS. The XRD and EDX data confirmed that the H_2S was removed in the form of FeS_2, FeS, $CaSO_4 \cdot 2H_2O$, sulfur, sulfide and bisulfide of Na. During the sulfidation reaction, the color of some RM changes from red to black, indicating that iron oxide was converted to iron sulfide. The black color in this case was an indicator of mineral sulfide compounds which indicated that some H_2S sorption and removal were occurred. The removal capacity of sulfidic filtrate was more as compared to the sulfidic red mud as revealed by thermogravimetric and EDX analysis.

Keywords: Red mud; Hydrogen sulfide; Iron oxide; Energy dispersive X-ray

1. Introduction

Red mud is a caustic waste material of bauxite ore processing for alumina extraction. Bayer process is commonly used for digestion of bauxite ore in a solution of conc. NaOH at a temperature of 150–230˚C under pressure. During the digestion process, aluminum reacts with NaOH to form soluble sodium aluminate leaving red mud slurry [1]. Red mud slurry is highly caustic having pH > 13, due to presence of NaOH and Na_2CO_3 (1–6%, w/w), these are expressed in terms of Na_2O [2,3]. The main constituents of red mud (% w/w) are: Fe_2O_3 (30–60%), Al_2O_3 (10–20%), SiO_2 (3–50%), Na_2O (2–10%), CaO (2–8%), and TiO_2 (trace–10%) [4].

Coal gasification generates large amounts of hydrogen sulfide gas which is responsible for a serious environmental problem [5,6]. H_2S gas is very corrosive, and highly toxic for the living organisms at relatively high concentration [7]. Furthermore, it is a constituent of sulfate aerosol which decreases droplet radius in cloud. The increase of aerosol concentration weakens rain fall and hydrological cycle in polluted cloud [8]. Several commercial techniques are available for the removal of H_2S, including aqueous NaCl [9], iron-based sorbents [10,11], activated carbon [12], FeOOH [13], Fe_2O_3, metal oxides [14], sewage sludge [15,16], and aqueous solutions [17]. However, there is always research for the development of effective and low-cost method.

Utilization of industrial wastes as a resource to solve the problem of another wastes provide economic benefit. Therefore, the removal of H_2S using red mud is one of the promising options for the reduction of industrial air pollution.

Removal of H_2S using aqueous RM takes place by the following reactions [7,17–21]:

$$H_2S(aq) + H_2O \leftrightarrow HS^-(aq) + H_3O^+ \quad (1)$$

$$H_2S(aq) + NaOH(aq) \leftrightarrow NaHS(aq) + H_2O(l) \quad (2)$$

$$H_2S(aq) + 2NaOH(aq) \leftrightarrow Na_2S + 2H_2O \quad (3)$$

$$Fe_2O_3 + 2H_2S + H_2 \rightarrow 2FeS + 3H_2O \quad (4)$$

$$[FeS] + H_2S \rightarrow [Fe{-}S{\rightarrow}SH_2] \rightarrow FeS_2 + H_2 \quad (5)$$

$$FeOOH(s) + 3HS^{-}(aq) + 3H^{-}(aq) \rightarrow FeS\,(s) + S^{0}(s) + 4H_2O\,(l) \quad (6)$$

$$CaCO_3(s) + H_2S\,(g) \rightarrow CaS\,(s) + H_2O\,(l) + CO_2\,(g) \quad (7)$$

$$CaS(s) + 2CO_2(g) + 2H_2O(l) \rightarrow CaSO_4{\cdot}2H_2O(s) + 2C(s) \quad (8)$$

The main objective of this study was to investigate the removal of H_2S using aqueous red mud at ambient conditions. In this work, red mud, sulfidic red mud, and sulfidic filtrate were characterized using the X-ray diffraction, scanning electron microscope, energy dispersive X-ray, thermogravimetric analysis, differential scanning calorimetric techniques, CHNS, FT-IR, etc.

2. Materials and methods

2.1. Materials

Red mud used in this study was obtained from R&D Laboratory of NALCO, Damanjodi, Orissa, India, in the form of dried–clay. Hydrochloric acid (HCl) used in this study was obtained from Merck and nitric acid (HNO_3) from Rankem. The H_2S gas (200 ppm) balanced by He gas was purchased from SKP Corporative Service Rourkela.

2.2. Materials preparation

The RM samples were air–dried, grounded in a mortar and pestle and stored in vacuum desiccators until used. The red mud suspension was prepared by mixing 5.0 g of red mud with 75

mL of distilled water in different plastic bottles of 150 mL to obtain a sufficient volume of slurry. The suspension was stirred through a magnetic stirrer for 24 h at constant speed ~5 s^{-1} for standard solid–liquid contact.

2.3. Materials characterization

The samples were oven-dried at a temperature of 110 ºC for 2 h before their analyses. The XRD pattern of the material and mineral composition were determined by using Philips X'Pert X-ray diffractometer with a Cu Kα radiation source in a 2θ range of 10° to 80º at a scanning rate of 2º min^{-1} and was analyzed using standard software provided with the instrument. The surface micro-morphology of materials was investigated using a scanning electron microscope (SEM) and element composition was analyzed using energy dispersive X-ray (EDX) by JOEL model JSM-6480LV (Japan). The pH measurements were made using a calibrated Orion 2 Star Bench top pH meter and electrical conductivity was measured using CM 138, EC-TDS analyzer. The pH and electrical conductivity were measured after centrifugation of suspensions (as prepared in Section 2.2) for 15 min at 3000 rpm and filtration were done using Whatman 42 filter paper. The parameters were measured by adding distilled water to the red mud at a solid to liquid ratio of 1:2.5 standard methods.

The thermogravimetric analysis and differential scanning calorimetry (TGA/DSC) analysis of air dried samples were carried out using NETZSCH STA 409C (Germany). In this analysis, 24–30 mg of sample was used. The sample was heated in an Al_2O_3 crucible at a heating rate of 10.0 ºC min^{-1} from 30 to 910 ºC. Sulfur content was determined by using varioELcube CHNS Elemental Analyzer, Germany. The O_2 gas was used as fuel, Helium gas was used as carrier gas and to provide inert atmosphere. The operating temperature of combustion tube and reduction tube were 1150 °C and 850 °C, respectively. The BET surface area of the sample was measured

at liquid nitrogen temperature using BET surface area analyzer (Quantachrome AUTOSORB–1, USA). Particle size of the red mud was measured using Master Sizer 33370-45 (Malverns, UK). The FT-IR spectra of the samples were obtained by using PerkinElmer FT-IR Spectrometer Spectrum RX-I. The spectrum was scanned from 4000 to 400 cm^{-1}. Samples were homogeneously crushed with anhydrous KBr in a ratio of 1:50. The powder was pressed at 10 tons cm^{-2} to make a translucent tablet for recording FT-IR spectra.

2.4. Batch experiments

Batch experiments were carried out at room temperature (25±2 ºC) using suspensions of different bottles as described in Section 2.2. The H_2S gas was passed through a rotameter at a gas flow rate of 50 mL min^{-1}, subsequently through a micro bubbles stone for 5, 10, 20, 30, 60 min into the suspensions of different bottles with an inlet and an outlet to vent the pressure. This experiment is referred as sulfidic reaction.

The suspension was stirred through a magnetic stirrer to increase their solubility at constant speed of ~5 s^{-1} for all the experimental tests reported here. After the reaction the suspension was centrifuged for 15 min at 3000 rpm and was air dried. It is referred as sulfided red mud (SRM). The filtrate was filtered through Whatman 42 filter paper and is referred as sulfidic filtrate (SF).

3. Results and discussion

3.1. Change of mineral composition

Particle size of the red mud was in the range of 0.1–160 μm. The BET-N_2 surface area, pore volume, pore diameter of RM were found to be 31.7 m^2 g^{-1}, 0.015 cm^3 g^{-1}, 18.20 Å, respectively (Table 1). Fig.1 shows the X-ray diffraction patterns of RM and SRM. From the XRD peaks of RM the following mineral phases were identified: hematite (α-Fe_2O_3), goethite (α-FeO(OH)), gibbsite(γ-$Al(OH)_3$), rutile/anatase (TiO_2), calcite ($CaCO_3$), sodalite: zeolite (I)

($1.08Na_2OAl_2O_31.68SiO_21.8H_2O$), quartz ($SiO_2$), sodium aluminum silicate ($Na(AlSiO_4)$), and magnetite (Fe_3O_4). However, a single weak peak of sodalite (labelled S) was showed by XRD. This may be due to the presence of less amount of sodalite in RM as compared to the other dominant crystalline mineral phases [1,3], which depends on the origin of RM. The XRD pattern of SRM confirmed the formation of iron pyrite (FeS_2) and iron sulfide (FeS), as referred from JCPDS file (42-1340, 76-0961) of X'Pert High Score software. But, most peaks that are assigned to FeS and FeS_2 in SRM seem to correspond almost exactly to peaks assigned to other components in RM. By using peak broadening technique of X'Pert High Score software of XRD analysis one can clearly differentiate among these peaks. However, in the compressed form of the graph (Fig. 1) they seem to be in exact position. FeS is extremely air sensitive and decomposes readily to FeS_2 and α-Fe_2O_3 even at room temperature. Therefore, no stoichiometric FeS was clearly detected by XRD [18]. The dominant crystal phase for calcined RM is α-Fe_2O_3. Furthermore, when H_2S concentration is low, only surface sulfide species will be formed because bulk sulfide is not thermally stable [19].

During the reaction brownish black precipitate of FeS was formed, due to the reaction between aqueous S(–II) and Fe(II). However, the rate of pyrite formation is slow relative to the rate of dissociation of FeS. Thus, FeS acts as continuous source for FeS_2 formation Eq. (5). In this reaction, H_2S acts as oxidizing agent with respect to [FeS] [20]. This reaction is possible, due to the attractive non-covalent interactions and the activation cost of bond rearrangement [21]. However, minimal changes are observed between the parent mineralogical species present in RM and SRM. Meanwhile, during the sulfidation reaction, the color of RM changes significantly from red to black, indicating that iron oxides (red) are converted to iron sulfide (black). The black color in this case is an indicator of mineral sulfide compounds which indicated that some

H_2S sorption and conversion did occur. The particle size of the material also plays crucial role. Since H_2S removal also depends on the available surface area.

3.2. Change of physical characteristics and chemical composition

The SRM and SF was oven dried at 60°C for 2 h before their SEM/EDX analysis. The SEM images of Fig. 2a (before reaction) and Fig. 2b (after reaction) show that the particles of RM have poorly-crystallized or amorphous forms, while the SRM contained smaller particles. This indicates that some mineral phase mainly calcite, sodalite contained in the RM are soluble in acidic environment. This may be responsible for decrease of rounded shape of aggregate in SRM [1]. However, RM is a mixture of fine and coarse particles. And some silicates often react with sodium aluminate in caustic suspension to form silicate mineral such as hydroxysodalite [1,22]. Furthermore, SEM analysis of SF (Fig. 2c) shows some long tubular particles, due to formation of $CaSO_4 \cdot 2H_2O$ [23,24] and several spots of unreacted NaOH.

Similarly, ~0.79%, and ~1.75% of S was accumulated in SRM and SF, respectively, as showed by the EDX analysis. The major elements such as Fe, Na, S, O, Ca, Si, and C were also present in SF (Fig. 2d, Table 2). This confirmed that H_2S could be removed by red mud, as sulfur is well dispersed in its surface. Furthermore, the oxides of red mud are acting as catalyst for the conversion of H_2S [7].

3.3. Thermogravimetric analysis (TGA)

The thermal decomposition behaviors of RM (Fig. 3a) show five steps for the weight loss. The first step occurs at 30–180 ºC (weight loss was about 3.34% of the total weight), due to the evaporation of water; the second one occur in the range of 180–390 ºC (6.75%), due to the loss of H_2O and also removal of H_2O from $Al(OH)_3$; third one occurred in the range of 390–900 ºC (1.86%), due to the release of CO_2 during decomposition of $CaCO_3$ to CaO. The DSC curve

shows two broad peaks centered at around 65 ºC and 291.5 ºC, corresponding to the physically adsorbed water and chemically adsorbed water, respectively [25,26].

The TG–DSC diagram of SRM (Fig. 3b) shows similar pattern to that of the RM. The weight loss in the region 30–180 ºC and 180–390 ºC was 2.35%, and 8.19%, respectively, due to the decomposition of water, and sulfur, respectively [15]. There is another step of weight loss in the region 390–900 ºC (0.95%), which may be due to the removal of some calcite [27]. Whereas, the decomposition of Fe_2S, FeS, and CaS occur at more than 1000 °C.

The TG–DSC diagram of sulfidic filtrate (Fig. 3c) shows different peaks to that of RM and SRM. The weight loss in the region 30–95 ºC and 95–150 ºC was 1.31%, and 23.78%, respectively, due to the loss of physically adsorbed H_2O and loss of H_2O from $CaSO_4{\cdot}2H_2O$, respectively [28]. The weight loss in the regions 150–775 ºC, 775–860 ºC, and 860–900 ºC was 4.66%, 1.45%, and 0.72%, respectively. The DSC curve shows two sharp peaks centered at 128.7 ºC and 844.8 ºC corresponding to the loss of H_2O from $CaSO_4{\cdot}2H_2O$ and decomposition of $CaCO_3$, respectively [27,28].

The total calculated amount of hydrogen sulphide retained in the SRM and SF were 1.7 and 0.4g/100g RM, respectively, as determined by CHNS analyzer at 1150°C. The H_2S removal at low temperatures (20–200°C) mainly occurs due to gas–solid reactions in a thin hydrated lattice of metal oxides (Eqs.4–8). Presence of iron selectively oxidizes the H_2S. As a result, H_2S is immobilized mainly in the form of sulfur compounds resulting from interactions of H_2S with iron oxides.

The removal capacity of red mud is comparable with the previously used materials by researchers shows the calculated result as: 1.31, 1.61, 1.63 and 1.83 g sulfur/100 g red soils Dadusan, Houli, Pingchen and Loupi, respectively [5], 1.44 g-S/100g activated carbon fiber [12],

456 mg H_2S/g sludge-based adsorbent and ~300–330 mg H_2S/g activated carbon when mixed with NaOH [16], whereas this study shows 2.1g H_2S/100g RM. The direct comparison with activated carbon and sludge-based adsorbent is difficult because the mechanism of absorption differs from adsorption. The removal capacity of H_2S depends on reaction conditions and materials used. Red mud should be used for removal of H_2S because it is an industrial waste and available with free of cost. So this is a low-cost material for removal of H_2S.

3.4. Variation of pH and electrical conductivity

Fig. 4a and c shows that the rapid decrease of pH of RM suspension from ~11.8 to ~7 is accompanied by decrease in electrical conductivity from ~7.2 to ~4.8 mS cm^{-1} for first 20 min of H_2S treatment, after that they slowly increases. Because, the reaction of H_2S with H_2O and HO^- in aqueous medium is very rapid, due to a permanent dipole moment and water like shape of H_2S, which acidify the RM suspension [15–17], Eqs. (1), (2), and (3). As a result, large amount of Ca– and Na–hydroxides/oxides were rapidly converted to sulfide and bisulfide species. Moreover, formation of sodium hydrogen sulphide is preferred over Na_2S when less amount of residual NaOH is available [16,17].

Furthermore, after centrifugation of H_2S treated RM suspension at pH ~7, the resultant pH of SRM was ~9.0. Similarly, pH of SF was ~10.1, due to the presence of large amount of basic element Na, Ca, Fe, and S (Fig. 4b). The pH of SRM was remained at ~9.0 instead of ~7.0 (Fig. 4a,b). This reversion of pH is due to the formation of FeS_2 and presence of unreacted OH^- ions, as Na^+ ion is a counter ion for H_2S gas to maintain the pH of suspension [20]. Since, silicates are able to exchange Na^+ ions with the suspension [2]. However, all this H_2S storage is not stable, depending on the reaction, produces OH^- and causing pH reversion. Also, due to more partial

pressure of hydrogen sulfide *in situ* than atmosphere and desilication reactions of treated RM are highly responsible.

3.5 Spectroscopy studies

Fig.5 shows the FT-IR spectra of H_2S-RM and RM. In both the spectra, the positions of the absorption bands are nearly similar. The relative intensities are more intense in the case of RM. The FT-IR absorption by RM showed a broad band at ~3140 cm^{-1} and a weak peak at ~1640 cm^{-1} due to the stretching vibrations of O–H bonds and H–O–H bending vibrations of interlayer adsorbed H_2O molecule, respectively. This reveals that by increasing the H_2S-RM sample temperature to 60 °C leads to the disappearance of all of the FT-IR bands due to H_2S absorption. It is also interesting to know that the characteristic S–H stretching vibration at 2562 cm^{-1}, because this band generally exhibits a very weak IR intensity and can sometimes be missed [29]. The absorption bands at ~1476 and ~1489 cm^{-1} are due to the stretching vibrations of C=O, confirmed the presence of carbonate groups. It confirmed that the fresh red mud was absorbed CO_2 from the atmosphere. Characteristic bands correspond to Si–O vibration were detected at ~993 cm^{-1} and for O–Si–O at ~803 cm^{-1} proved the presence of silicate groups. Peaks at ~544 and ~466 cm^{-1} are due to the bending vibration of Si–O–Al and stretching vibrations of Fe–O bonds respectively [30].

H_2S can react with alkaline materials and be removed from the gas phase. As a gas molecule diffuses through a porous media, gas molecules adsorbed to the surfaces of red mud materials by physisorption and chemisorptions. Because of their alkaline nature, iron oxide, NaOH, $Ca(OH)_2$ can react with H_2S and subsequently converted to sulfide minerals through reactions Eqs. (1–6). Alkaline fine red mud has greater capabilities in conversion of H_2S as compared to the clay and

sandy soils [31]. In liquid phases, absorption of H_2S is more by NaOH as compared to FeOOH, Fe_2O_3 [32,33], through dissolution and precipitation [34].

4. Conclusions

In this preliminary study, H_2S gas was removed by using aqueous red mud at ambient conditions. The XRD, EDX analysis results showed that the hydrogen sulfide was removed in the form of FeS_2, FeS, S, and sulfide minerals. During the sulfidation reaction, RM changes from red to black, indicating that some iron oxide was converted to iron sulfide. Furthermore, the red mud used here is produced as a by-product in the alumina industry and currently have no economic value. They could be used directly, therefore no additional manufacturing cost. Hence, the waste red mud can be used for the removal of air pollutant H_2S from industrial emission.

Acknowledgements

The authors would like to thank CSIR and MHRD, New Delhi, India for financial support. The authors also thank NIT, Rourkela for providing necessary facilities.

References

[1] T. Newson, T. Dyer, C. Adam, S. Sharp, Effect of structure on the geotechnical properties of bauxite residue, J. Geotech. Eng. 132(2) (2006) 143–151.

[2] E. Fois, A. Lallai, G. Mura, Sulfur dioxide absorption in a bubbling reactor with suspensions of Bayer red mud, Ind. Eng. Chem. Res. 46 (2007) 6770–6776.

[3] R.C. Sahu, R.K. Patel, B.C. Ray, Neutralization of red mud using CO_2 sequestration cycle, J. Hazard.Mater. 179 (2010) 28–34.

[4] A. Collazo, M.J. Cristobal, X. R. Novoa, G. Pena, M. C. Perez, Electrochemical impedance spectroscopy as a tool for studying steel corrosion inhibition in simulated concrete environments-red mud used as rebar corrosion, J. ASTM. Int. 3(2) (2006) 1–10.

[5] T-H. Ko, H. Chu, H-P. Lin, C-Y. Peng, Red soil as a regenerable sorbent for high temperature removal of hydrogen sulfide from coal gas, J. Hazard. Mater. B136 (2006) 776–783.

[6] J.B. Chung, J.S. Chung, Desulfurization of H_2S using cobalt-containing sorbents at low temperatures, Chem. Eng. Sci. 60 (2005) 1515–1523.

[7] M.A. Shields, N.I. Dowling, P.D. Clark, Catalytic H_2S conversion and SO_2 production over iron oxide and iron oxide/γ-Al_2O_3 in liquid sulfur, Ind. Eng. Chem. Res. 46 (2007)7721–7728.

[8] V. Ramanathan, P.J. Crutzen, J.T. Kiehl, D. Rosenfeld, Aerosols, climate, and the hydrological cycle, Science. 294 (2001) 2119.

[9] Z. Duan, R. Sun, R. Liu, C. Zhu, Accurate thermodynamic model for the calculations of H_2S solubility in pure water and brines, Energy & Fuels. 21 (2007) 2056–2065.

[10] W. Xie, L. Chang, D. Wang, K. Xie, T. Wall, J. Yu, Removal of sulfur at high temperatures using iron-based sorbents supported on fine coal ash, Fuel 89 (2010) 868–873.

[11] N.N. Nassar, M.M. Husein, P. Pereira-Almao, Ultrasispersed particles in heavy oil: Part II, sorption of $H_2S_{(g)}$, Fuel Pro. Tech. 91 (2010) 169-174.

[12] J.J. Choi, Oxidative removal of malodorous volatile sulfur compounds by air over a activated carbon fiber, J. Ind. Eng. Chem. 3 (1997) 56–62.

[13] S. Peiffer, W. Gade, Reactivity of ferric oxide toward H_2S at low pH, Environ. Sci. Technol. 41 (2007) 3159–3164.

[14] X.M. Meng, W.D. Jong, AH.M. Verkooijen, Thermodynamic analysis and kinetics model of H_2S sorption using different sorbents, Env. Prog. & Sus. Ener. 28 (2009) 360–371.

[15] A. Bagreev, S. Bashkova, D.C. Locke, T.J. Bandosz, Sewage sludge-derived materials as efficient adsorbents for removal of hydrogen sulfide, Environ. Sci. Technol. 35 (2001)1537–1543.

[16] A. Ros, M.A. Lillo-Rodens, C. Canals-Batlle, E.Fuente, M.A. Montes-Moran, M.J. Martin, A. Linares-Solano, A new generation of sludge-based adsorbents for H_2S abatement at room temperature, Environ. Sci. Technol. 41 (2007) 4375–4381.

[17] J. Boniface, Q. Shi, Y.Q. Li, J.L. Cheung, O.V. Rattigan, P. Davidovits, Utake of gas- phase SO_2, H_2S, and CO_2 by aqueous solutions, J. Phys. Chem. A 104 (2000) 7502–7510.

[18] L. Zhang, J-M. M. Millet, U.S. Ozkan, Deactivation characteristics of Fe–Al–Cu water–gas shift catalysts in the presence of H_2S, J. Mol. Catal. A: Chem. 309 (2009) 63–70.

[19] Z. Cheng, M. Liu, Characterization of sulfur poisoning of Ni–YSZ anodes for solid oxide fuel cells using *in situ* Raman microscopy, Solid State Ionics 178 (2007) 925–935.

[20] D. Rickard, G.W. Luther, Chemistry of iron sulfides, Chem. Rev. 107 (2007) 514–562.

[21] B.A. Ellingson, D.G. Truhlar, Explanation of unusual temperature dependence of the atmospherically important $OH + H_2S \rightarrow H_2O + HS$ reaction and prediction of rate constant at combustion temperatures, J. Am. Chem. Soc. 129 (2007) 12765–12771.

[22] S.J. Palmer, R.L. Frost, T. Nguyen, Hydrotalcites and their role in coordination of anions in Bayer liquors: anion binding in layered double hydroxides, Coordi. Chem. Rev. 253 (2009) 250–267.

[23] J. Li, G. Li, Y. Yu, The influence of gypsum water-proofing additive on gypsum crystal growth, Materials Letters. 61 (2007) 872–876.

[24] N.R. Mbhele, W.V.D. Merwe, J.P.Maree, D. Theron, Recovery of sulphur from waste gypsum, International Mine Water Conference, (2009) 622-630.

[25] Y.N. Zhang, Z.H. Pan, Characterization of red mud thermally treated at different temperature, J. Jinan University (Sci & Tech.) 19 (4) (2005) 293–297.

[26] R.C. Sahu, R.K. Patel, B.C. Ray, Adsorption of Zn(II) on activated red mud: Neutralized by CO_2, Desalination. 266 (2011) 93–97.

[27] R. Bassilakis, Y. Zhao, P.R. Solomon, M.A. Serio, Sulfur and nitrogen evolution in the Argonne coals: experimental and modeling, Energy & Fuel. 7 (1993) 710–720.

[28] C.G. Julia, C.P. Bonafe, The use of natural earths in picture: study and differentiation by thermal analysis, Thermochimica Acta 413 (2004) 185–192.

[29] H.Y. Huang, R.T. Yang, Amine-grafted MCM-48 and silica xerogel as superior sorbents for acidic gas removal from natural gas, Ind. Eng. Chem. Res. 42 (2003) 2427–2433.

[30] R.C. Sahu, R.K. Patel, B.C.Ray, Utilization of activated CO_2–neutralized red mud for removal of arsenate from aqueous solutions, J. Hazard. Mater. 179 (2010) 1007–1013.

[31] C. Plaza, Q. Xu, T. Townsend, G. Bitton, M. Booth, Evaluation of alternative landfill over soils for attenuating hydrogen sulfide from construction and demolition (C&D) debris landfills, J. Env. Mang. 84 (2007) 314–322.

[32] M.M. Husein, L. Patruyo, P. Pereira-Almao, N.N. Nassar, Scavenging $H_2S_{(g)}$ from oil phases by means of ultradispersed sorbents J. Colloid Interface Sci. 342 (2010) 253–260.

[33] T.K. Tseng, H.C. Chang, H. Chu, H.T. Chen, Hydrogen sulfide removal from coal gas by the metal-ferrite sorbents made from the heavy metal wastewater sludge, J. Hazard. Mater. 160 (2008) 482–488.

[34] K-D. Jung, O-S. Joo, S-H. Cho, S-H. Han, Catalytic wet oxidation of H_2S to sulfur on Fe/MgO catalyst, Appl. Catal. A: Gen. 240 (2003) 235–241.

List of Figures

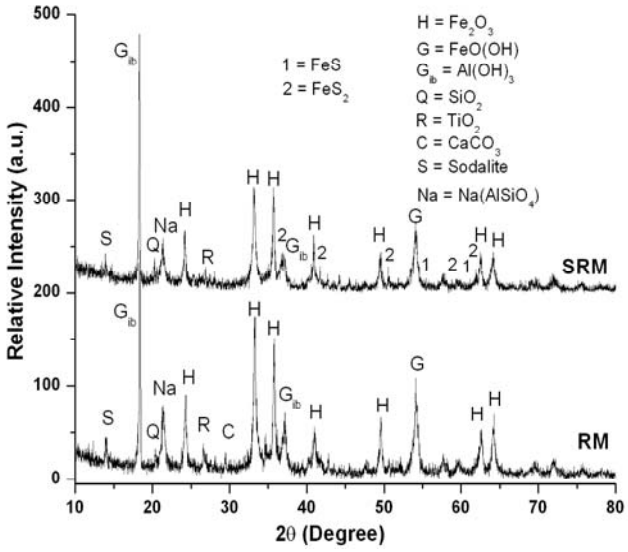

Fig. 1.

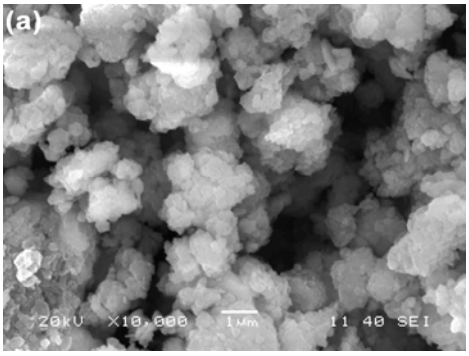
(a)
20kV X10,000 1μm 11 40 SEI

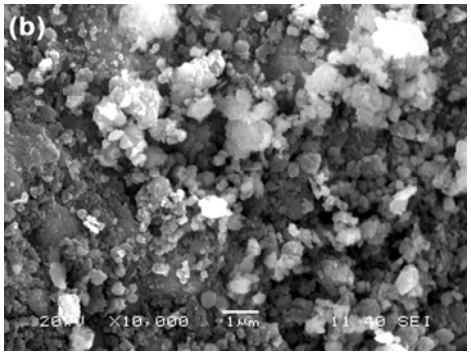
(b)
20kV X10,000 1μm 11 40 SEI

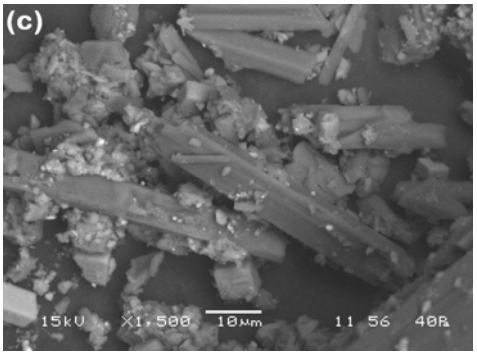
(c)
15kV X1,500 10μm 11 56 40R

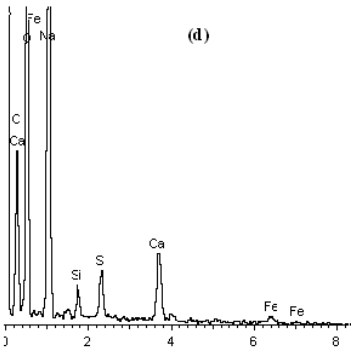
(d)
C
Ca
O
Fe
Na
Si
S
Ca
Fe
Fe
0
2
4
6
8

Fig. 2.

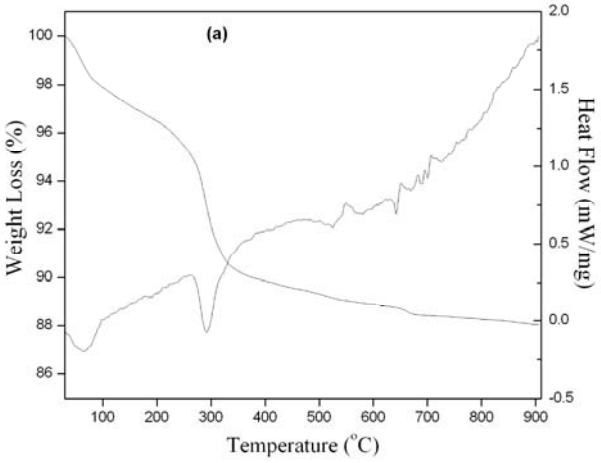
(a)
Weight Loss (%)
Heat Flow (mW/mg)
Temperature (°C)
100
98
96
94
92
90
88
86
2.0
1.5
1.0
0.5
0.0
-0.5
100
200
300
400
500
600
700
800
900

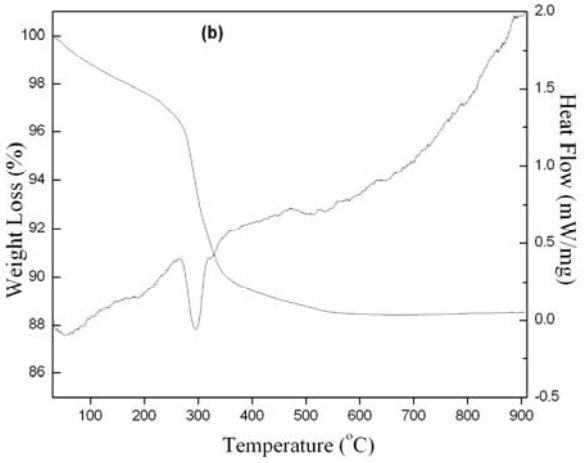
(b)
Weight Loss (%)
Heat Flow (mW/mg)
Temperature (°C)
100
98
96
94
92
90
88
86
2.0
1.5
1.0
0.5
0.0
-0.5
100
200
300
400
500
600
700
800
900

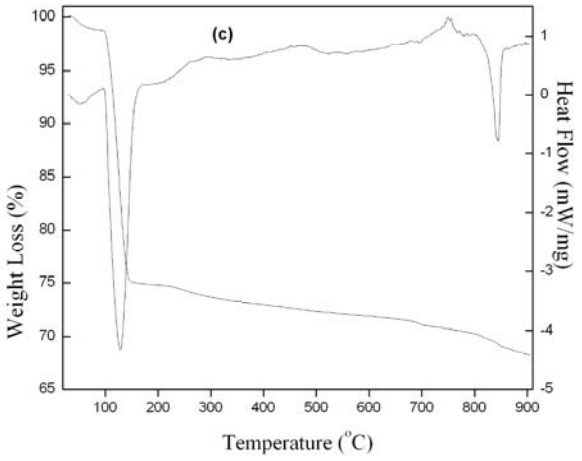

Fig.3.

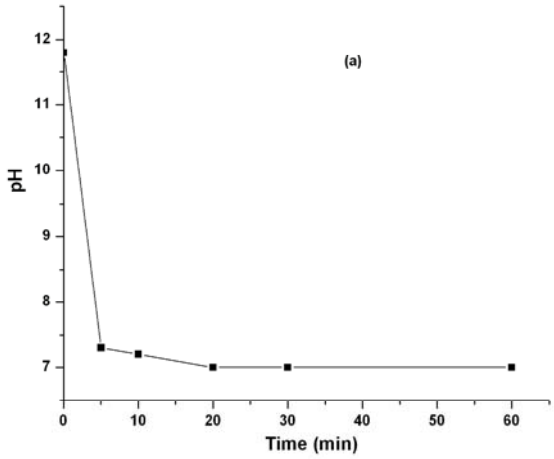

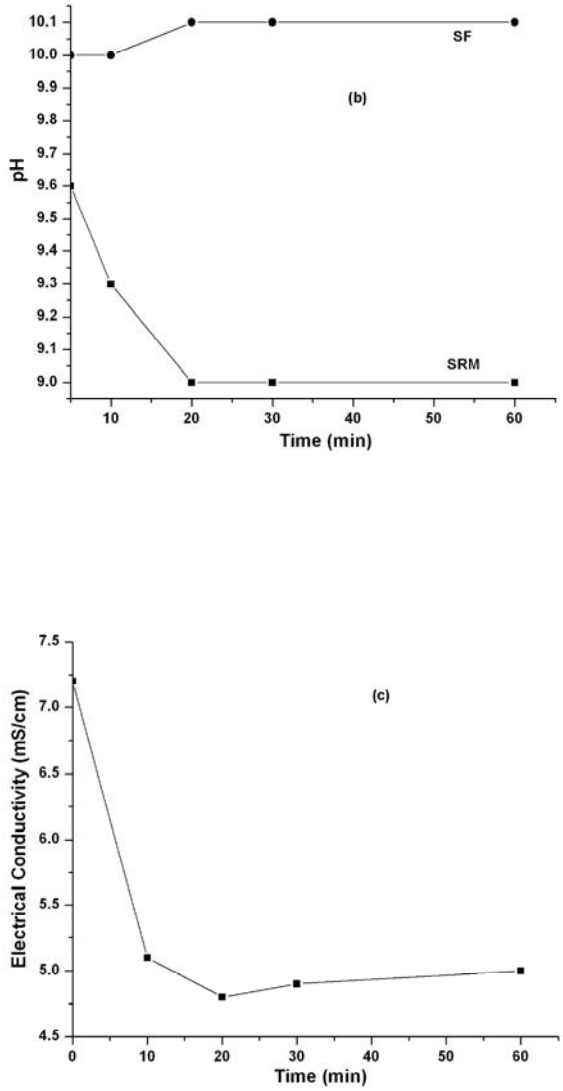

Fig. 4.

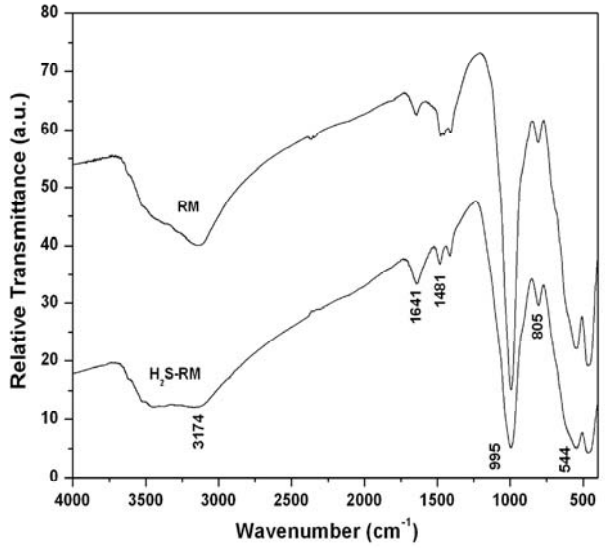

Fig. 5.

List of Tables

Table 1. Physical properties of red mud.

Table 2. Major elements composition (%w/w) of RM, SRM and SF in average as determined by energy dispersive X-ray.

Table 1.

S_{BET}	31.7 $m^2 g^{-1}$
Particle size	0.1–160 μm
Pore volume	0.015 $cm^3 g^{-1}$
Pore diameter	18.20 Å

Table 2.

Major elements	RM	SRM	SF
C	1.97	1.03	18.38
O	31.86	35.81	59.55
Na	4.30	0.95	14.32
Al	5.86	4.27	---
Si	3.83	1.08	1.00
Ca	0.74	---	3.75
Ti	1.82	0.75	---
Fe	47.62	53.01	1.25
Zr	2.00	2.31	---
S	---	0.79	1.75
Total	100.00	100.00	100.00